Chem. Pap. (2017) 71:1235–1248
DOI 10.1007/s11696-016-0117-0

ORIGINAL PAPER

Supramolecular adducts of native and permethylated β-cyclodextrins with (2,2′-dipyridylamine)chlorido(1,4,7-trithiacyclononane)ruthenium(II) chloride: solid-state and biological activity studies

Susana S. Braga[1] · Joana Marques[2] · José A. Fernandes[2] · Filipe A. Almeida Paz[2] · M[a] Paula M. Marques[3,4] · Teresa M. Santos[2] · Artur M. S. Silva[1]

Received: 26 October 2016 / Accepted: 21 December 2016 / Published online: 6 February 2017

Abstract The complex [([9]aneS$_3$)Ru^{II}(dipa)Cl]Cl (**1**, where dipa = 2,2′-dipyridylamine) was included into native β-cyclodextrin (β-CD) and permethylated β-CD (TRIMEB) by co-dissolution followed by solvent removal. Two adducts were obtained with a 1:1 host:guest stoichiometry. Solid-state studies of the guest comprised collecting the single-crystal structure of its 3.5 hydrate form and also powder diffraction on the remaining bulk material, showing it is isotypical with the harvested crystal for X-ray analysis. Solid-state studies of the cyclodextrin adducts were carried out by powder X-ray diffraction (PXRD), thermogravimetric analysis (TGA), $^{13}C\{^1H\}$ CP/MAS NMR and FTIR spectroscopies. Biological studies on **1** and its adducts comprised the evaluation of the shift caused by **1** on the melting temperature of DNA (ΔT_m), as well as the evaluation of cytotoxicity by the MTT assay on the osteosarcoma MG-63 cell line.

Keywords Cyclodextrin inclusion · Host–guest chemistry · Ru(II)-dipyridylamine complex · Solid-state · Osteosarcoma chemotherapy

Introduction

Cyclodextrins (CDs) are cyclic oligosaccharides obtained from renewable sources, typically corn or potato starch (Biwer et al. 2002). Recently, the preparation of CDs using starch from environmentally friendly species such as the sago palm (Charoenlap et al. 2004) or cassava (Szerman et al. 2007) was reported with promising results which make way for a cheaper and more sustainable production. The most abundant native cyclodextrins are α-CD, β-CD and γ-CD, having six to eight 1,4-linked α-D-glucose units, respectively, all in the chair conformation, giving CDs the shape of a truncated cone. Such combination of shape and geometry empowers CDs with unique properties: on the one hand, the hydroxyl terminal residues face the edges making them water soluble; on the other, protons of carbons 3 and 5 face the inner cavity, allowing the CDs to host hydrophobic molecules. A quasi-endless variety of CD inclusion compounds with organic guests is described. Inclusion improves the guest's solubility, flavour or aroma, the biological action, or the stability to light and heat. The applications cover a wide range of fields, with highlights to pharmaceuticals, cosmetics and food.

Cyclodextrin inclusion compounds with metal complexes and organometallic compounds are less explored than those with organic guests. Nonetheless, a fair number of these have demonstrated interesting properties, which are brought about by the host–guest synergistic action (Hapiot et al. 2006; Prochowicz et al. 2016). Cyclodextrins, besides their solubilising effect (Pirvu et al. 2013), act as

Electronic supplementary material The online version of this article (doi:10.1007/s11696-016-0117-0) contains supplementary material, which is available to authorized users.

✉ Susana S. Braga
sbraga@ua.pt

[1] QOPNA Research Unit, Department of Chemistry, University of Aveiro, 3810-193 Aveiro, Portugal

[2] Department of Chemistry, CICECO-Aveiro Institute of Materials, University of Aveiro, 3810-193 Aveiro, Portugal

[3] "Molecular Physical-Chemistry" R&D Unit, Faculty of Science and Technology, University of Coimbra, Coimbra, Portugal

[4] Department of Life Sciences, Faculty of Science and Technology, University of Coimbra, Coimbra, Portugal

second-sphere ligands, protecting the metallo-organic guest against hydrolytical instability (Braga et al. 2001) and thermal (Braga et al. 2014) or electrical degradation (Braga et al. 2008). CDs were shown to increase the biological activity of some metallo-organic guests, namely the antioxidant action (Martin et al. 2003), the cytotoxicity and the selectivity (Paz et al. 2010). Regarding the guests, ruthenium complexes have conquered a very important place. Nowadays the applications of cyclodextrin-ruthenium supramolecular systems are largely spread across many fields. Examples include molecular devices such as single or polynuclear fluorescence sensors (Zhang et al. 2015; Chen et al. 2013) and CD-stabilised Ru(II) photosensitizers for dye-sensitized solar cells (Farras et al. 2016) or cyclodextrin metallosurfactants (M = Ru(II)) for gene therapy (Lebron et al. 2015; Iza et al. 2015). In antitumoral chemotherapy, ruthenium complexes make a strong claim as alternatives to platin compounds, for their more versatile ligand-exchange abilities, redox properties (+2 and +3 oxidation states accessible in vivo) and octahedral geometry (instead of planar four-coordinated Pt) (Bergamo et al. 2012). Their biological properties were first recognised in the 1950s by Dwyer et al. (1952), who later found bactericidal (Dwyer et al. 1969) and antitumoral (Dwyer et al. 1965) actions for simple Ru(II)$(N,N')_3$ complexes (N,N′ = 2,2′-bipyridine, 1,10-phenanthroline and 3,4,7,8-tetramethyl-1,10-phenanthroline). In the 1980s, Clarke designed chlorido-ammine complexes of Ru(II) and Ru(III) as cisplatin mimics (Clarke 1980, 2003) and the late 1990s witnessed the dawn of two Ru(III) antitumoral drug candidates, NAMI-A and KP1019. NAMI-A (imidazolium [*trans*-$Ru^{III}Cl_4$(DMSO)imidazole]) (Mestroni et al. 1996; Sava et al. 1998), displays anti-metastatic action in vitro, likely by interactions with actin-type proteins on the cell surface (Sava et al. 2004; Gava et al. 2006), or with extracellular collagen (Sava et al. 2003; Casarsa et al. 2004). It was the first ruthenium complex to enter clinical trials, but it had a poor low performance in phase I requiring co-administration in combination with gemcitabine for phase II studies. Such combination was only moderately tolerated and less active in non-small cell lung cancer patients after first line treatment than gemcitabine alone, which leaves NAMI-A with an uncertain future role as a drug (Leijen et al. 2015). KP1019 (indazolium [*trans*-$Ru^{III}Cl_4$bisindazole]) (Peti et al. 1999) has in vitro apoptotic activity against colorectal cancer (Kapitza et al. 2005) and has successfully overcome phase I clinical trials (Lentz et al. 2009; Henke et al. 2009) being now under phase II studies. The last two decades were prolific in studies on Ru(II) anticancer drug candidates, both inorganic polypyridyl complexes and organometallics with arene facial ligands. These include the RAPTA family (RAPTA-C = $[Ru^{II}(\eta^6$-*p*-cymene)(PTA)$Cl_2]$, PTA = 1,3,5-triaza-7-phosphatricyclo-[3.3.1.1] decanephosphine), of which a few have completed preclinical trials (Morris et al. 2001; Murray et al. 2014, 2016; Allardyce and Dyson 2016; Scolaro et al. 2008), and RM175 ($[Ru(\eta^6$-biphenyl)(ethylenediamine)$Cl]^+$) (Aird et al. 2002; Hayward et al. 2005; Bergamo et al. 2010). Within the inorganic complexes, emerging families are Ru(II/III) dithiocarbamates (Nardon et al. 2016) and Ru(II) [9]aneS_3 complexes ([9]aneS_3 = 1,4,7-trithiacyclononane), having a facial tridentate ligand in place of the arene (Goodfellow et al. 1997; Santos et al. 2001; Rilak et al. 2014). We have developed and tested a few of these complexes (Marques et al. 2012, 2014), with highlight to [([9]aneS_3)Ru^{II}(phpz)Cl] (phpz = 5-(2-hydroxyphenyl)-3-[(4-methoxystyryl)-pyrazole), having high cytotoxicity against prostate cancer (PC-3) and breast cancer (MDA-MB-231) cells (Marques et al. 2014). Further modification of Ru(II)-[9]aneS_3 complexes by placing β-CD and its derivatives in a second sphere of coordination was studied for [([9]aneS_3)Ru^{II}(glycine)Cl] (Marques et al. 2009a) and [([9]aneS_3)Ru^{II}(1,10-phenanthroline)Cl]Cl (Marques et al. 2009b). The later exhibits increased biocidal activity against a series of bacteria when encapsulated with heptakis(2,3,6-*tris*-O-methyl)-β-CD (TRIMEB).

The present paper reports the inclusion of the complex [([9]aneS_3)Ru^{II}(dipa)Cl]Cl, which bears the amine ligand 2,2′-dipyridylamine (hereafter coined as dipa). Due to its higher hydrophilicity when compared to phen or bpy, dipa allows to prepare more soluble, and thus, more active ruthenium complexes (Romain et al. 2010). In addition, the structure of dipa has increased conformational freedom in comparison with those of 2,2′bipyridine or 1,10-phenanthroline and derivatives, maintaining a non-planar geometry even after coordination to ruthenium. These two features of dipa are expected to influence the overall biological activity of [([9]aneS_3)Ru^{II}(dipa)Cl]Cl, making it worthy of investigation.

Experimental

Materials and methods

β-CD was kindly donated by Roquette (France), and heptakis-2,3,6-tri-*O*-methyl-β-CD was obtained from Cyclolab (Hungary). Ruthenium trichloride was purchased from Alfa-Aesar (Spain) and 1,4,7-trithiacyclononane ([9]aneS_3) was purchased from Aldrich (Spain). All air-sensitive operations were carried out using standard Schlenk techniques under nitrogen.

Microanalyses for C, H, N and S were performed at the Department of Chemistry of the University of Aveiro (by M. Marques), and Ru was determined by ICP-OES at the

Central Laboratory for Analysis, University of Aveiro (by L. Soares).

Powder X-ray diffraction data of the bulk compounds were collected at ambient temperature on a X'Pert MPD Philips diffractometer (Cu $K\alpha_{1,2}$ X-radiation, $\lambda_1 = 1.540598$ Å and $\lambda_2 = 1.544426$ Å), equipped with a X'Celerator detector and a flat-plate sample holder in a Bragg–Brentano para-focusing optics configuration (40 kV, 50 mA). Intensity data were collected by the step-counting method (step 0.02°), in continuous mode, in the ca. $3.0 \leq 2\theta \leq 50.0°$ range.

TGA studies were carried out using a Shimadzu TGA-50 system using a heating rate of 5 °C/min, under air atmosphere, with a flow rate of 20 mL/min. The sample holder was a 5 mm ∅ platinum plate and the sample mass was typically between 1 and 5 mg.

FTIR spectra (range 4000–380 cm^{-1}) were collected as KBr pellets using a Unican Mattson Mod 7000 FTIR spectrophotometer by averaging 64 scans at a maximum resolution of 2 cm^{-1}. In a typical preparation, 2 mg of sample were mixed in a mortar with 200 mg of KBr (Sigma-Aldrich, ≥99%). Raman spectra were collected in a Bruker RFS 100/S spectrometer equipped with an Nd:YAG laser (1064 nm), working between 30–50 mW at the sample position.

Solid-state nuclear magnetic resonance spectra with $^{13}C\{^1H\}$ cross-polarization and magic angle spinning (CP/MAS NMR) were recorded at 125.72 MHz on a (11.7 T) Bruker Avance 500 spectrometer, with an optimised π/2 pulse for ^1H of 4.5 μs, 2 ms contact time, a spinning rate of 7 kHz and 12 s recycle delays. Chemical shifts are quoted in parts per million from tetramethylsilane.

UV/Vis absorption spectra were collected using a GBC Cintra 500 UV–Visible spectrophotometer equipped with a temperature controller (GBC Thermocell).

Synthetic and inclusion procedures

*[([9]aneS$_3$)Ru^{II}(dipa)Cl]Cl (**1**)*

This compound was prepared by adapting a literature procedure (see Scheme 1) (Madureira et al. 2000). The two-step synthesis and structural description of the precursor [([9]aneS$_3$)Ru^{II}(DMSO)Cl$_2$] is previously published (Marques et al. 2009b; Landgrafe and Sheldrick 1994). A solution of 43.1 mg (0.252 mmol) of dipa and 107.5 mg (0.25 mmol) of [([9]aneS$_3$)Ru^{II}(DMSO)Cl$_2$] in 20 ml dry ethanol was refluxed for 1 h. The isolation of the reaction product is achieved by precipitation with NH_4PF_6 to afford a yellow solid of formula [([9]aneS$_3$)Ru^{II}(dipa)Cl]PF_6. The new crystalline chloride complex was obtained by performing the anion exchange with chloride. The yellow solid was re-dissolved in tetrabuthylammonium chloride and then precipitated over acetone to yield [([9]aneS$_3$)Ru^{II}(dipa)Cl]Cl.

Anal. Calc. for $(C_{16}H_{21}S_3N_3RuCl_2)\cdot 1.2H_2O$ (545.1): C, 35.26; H, 4.33; N, 7.75; S, 17.61; Ru, 18.64. Found: C, 35.18; H, 5.01; N, 7.67; S, 16.42; Ru, 18.04%.

FTIR and liquid-state ^1H NMR signals are coherent with those previously published for **1** (Madureira et al. 2000).

$^{13}C\{^1H\}$ CP/MAS NMR: 153.3 (dipa, C_a), 151.9 (dipa, $C_{a'}$), 140.7, 139.4, 135.6 (dipa C_{c+e}), 121.9, 119.5 (dipa, $C_{d+d'}$), 114.8, 113.5 (dipa, $C_{b+b'}$), 38.5, 33.8, 30.0 ([9]aneS$_3$) ppm (see Scheme 2 for carbon labelling of the dipa ligand).

*β-CD·[([9]aneS3)RuII(dipa)Cl]Cl·xH$_2$O (**2**)*

An aqueous solution (4 mL) of β-CD (74 mg, 0.0517 mmol) was treated with 30 mg (0.056 mmol) of **1**. The mixture was stirred for 10 min at ambient temperature and then subjected to snap-freezing using liquid nitrogen. Solvent was removed by freeze-drying to obtain a voluminous pale yellow solid.

Anal. Calc. for $(C_{42}H_{70}O_{35})\cdot(C_{16}H_{21}S_3N_3RuCl_2)\cdot 6H_2O$ (1766.6): C, 39.43; H, 5.88; N, 2.37; S, 5.44; Ru, 5.72. Found: C, 39.42; H, 6.08; N, 2.41; S, 4.67; Ru, 5.66%.

FTIR (KBr, cm^{-1}): nu(tilde) = 3373 s, 2927 m, 2854 sh, 1633 m, 1580 m, 1560 w, 1528 w, 1473 s, 1434 m, 1414 m, 1356 m, 1337 m, 1299 m, 1273 w, 1261 w, 1240 m, 1159 s, 1123 m, 1080 s, 1027 vs, 1000 s, 947 m, 935 m, 910 w, 848 m, 827 w, 775 m, 763 m, 709 m, 609 m, 576 m, 532 m, 440 w, 420 w, 402 w, 369 vw, 355 vw, 335 vw, 329 vw, 324 vw, 303 w, 289 w.

$^{13}C\{^1H\}$ CP/MAS NMR: 154.1, 152.1, 128.9, 140.9, 139.8, 122.2, 119.7, 115.2, 113.7 (guest, dipa), 103.1,

Scheme 1 .

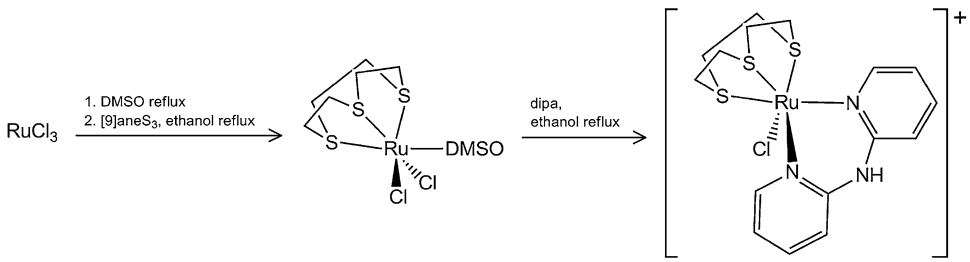

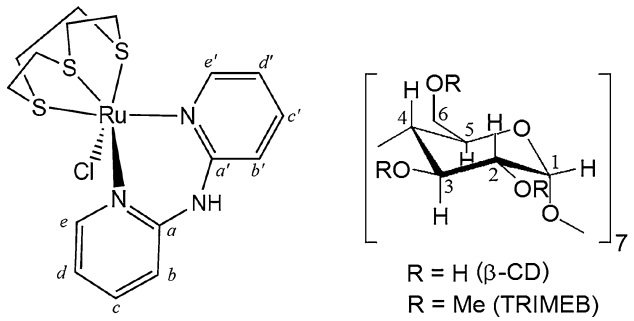

Scheme 2 .

102.4 (β-CD, C1), 84.0, 81.5, 78.4 (β-CD, C4), 73.5 (β-CD, C2,3,5), 63.6, 62.1, 60.0 (β-CD, C6), 34.2 (guest, [9]aneS$_3$) ppm (see Scheme 2 for cyclodextrin carbon numbering).

*TRIMEB·[([9]aneS$_3$)Ru^{II}(dipa)Cl]Cl·5H$_2$O (**3**)*

A solution of TRIMEB (158.2 mg, 0.11 mmol) in ethanol (7 mL) was treated with solid **1** (59 mg, 0.111 mmol), stirred for 1 h and then subject to evaporation to remove the solvent.

Anal. Calc. for $(C_{63}H_{112}O_{35})\cdot(C_{16}H_{21}S_3N_3RuCl_2)\cdot 5(H_2O)$ (2043.1): C, 46.44; H, 7.05; N 2.05; S, 4.71; Ru, 4.95. Found: C, 46.46; H, 7.05; N 1.82; S, 4.29; Ru, 5.12%.

FTIR (KBr, cm^{-1}): nu(tilde) = 3423 s, 2974 s, 2930 s, 2830 m, 1633 m, 1579 m, 1474 s, 1458 m, 1413 m, 1365 m, 1355 m, 1320 m, 1303 m, 1259 w, 1233 m, 1195 s, 1163 vs, 1140 vs, 1108 vs, 1065 vs, 1041 vs, 1020 vs, 970 m, 953 m, 935 w, 909 w, 859 w, 826 w, 771 w, 706 w, 668 m, 574 m, 559 m, 531 m, 494 w, 420 vw, 372 vw, 344 w, 302 m.

^{13}C{^{1}H} CP/MAS NMR: 153.9, 152.4, 141.1, 122.5, 119.9, 115.3, 114.2 (guest, dipa), 99.7 (TRIMEB, C1), 83.1 (TRIMEB, C2,3,4), 71.9 (TRIMEB, C5,6), 60.9 (sh), 59.1 (TRIMEB, O–CH$_3$), 34.4 (guest, [9]aneS$_3$) ppm (see Scheme 2 for numbering).

Single-crystal X-ray diffraction studies

Single crystals of [([9]aneS$_3$)Ru^{II}(dipa)Cl]Cl·3.5H$_2$O (**1**) were manually harvested from the crystallization vials and immediately immersed in highly viscous FOMBLIN Y perfluoropolyether vacuum oil (LVAC 140/13, Sigma-Aldrich) to avoid degradation caused by the evaporation of the solvent, then mounted on Hampton Research Cryo-Loops. These operations were performed with the help of a Stemi 2000 stereomicroscope equipped with Carl Zeiss lenses (Kottke and Stalke 1993). Data were collected on a Bruker X8 Kappa APEX II CCD area-detector diffractometer (Mo Kα graphite-monochromated radiation, $\lambda = 0.71073$ Å) controlled by the APEX2 software package (APEX2 2006) and equipped with an Oxford Cryosystems Series 700 cryostream monitored remotely using the software interface Cryopad (Cryopad v1.451 2006). Images were processed using the software package SAINT+ (SAINT+ v7.23a 1997), and data were corrected for absorption by the multiscan semi-empirical method implemented in SADABS (Sheldrick 1998).

The structure was solved using the Patterson synthesis algorithm implemented in SHELXS-97 (Sheldrick 1997a, 2008), which allowed the immediate location of the most occupied Ru^{2+} position and most of the heaviest atoms. The remaining non-hydrogen atoms were located from difference Fourier maps calculated from successive full-matrix least-squares refinement cycles on F^2 using SHELXL-2014/7 (Sheldrick 1997a, b). The crystal

Table 1 Crystal data collection and structure refinement details for [([9]aneS$_3$)Ru^{II}(dipa)Cl]Cl·3.5H$_2$O (**1**)

Formula	$C_{16}H_{21}Cl_2N_3RuS_3\cdot 3.5(H_2O)$
Formula weight	586.56
Temperature (K)	150(2)
Crystal system	Orthorhombic
Space group	*Iba*2
a/Å	19.542(2)
b/Å	31.505(4)
c/Å	7.5118(9)
Volume (Å^3)	4624.8(10)
Z	8
D_c (g cm^{-3})	1.685
μ(Mo-Kα) (mm^{-1})	1.205
Crystal size (mm)	0.09 × 0.03 × 0.01
Crystal type	Yellow needle
θ range (°)	2.08–29.11
Index ranges	$-23 \le h \le 26$, $-43 \le k \le 14$, $-8 \le l \le 10$
Reflections collected	21762
Independent reflections	5158 [$R_{int} = 0.1156$]
Completeness to $\theta = 29.11°$	99.8%
Final *R* indices [$I > 2\sigma(I)$][a,b]	$R1 = 0.0993$, $wR2 = 0.1914$
Final *R* indices (all data)[a,b]	$R1 = 0.1485$, $wR2 = 0.2038$
Weighting scheme[c]	$m = 0.0512$
	$n = 0.000$
Largest diff. peak and hole	0.824 and −1.601 eÅ^{-3}

[a] $R1 = \sum ||F_o| - |F_c|| / \sum |F_o|$

[b] $wR2 = \sqrt{\sum [w(F_o^2 - F_c^2)^2] / \sum [w(F_o^2)^2]}$

[c] $w = 1/[\sigma^2(F_o^2) + (mP)^2 + nP]$ where $P = (F_o^2 + 2F_c^2)/3$

structure was ultimately found to be highly disordered, with the whole ion of $[([9]aneS_3)Ru^{II}(dipa)Cl]^+$ distributed over two opposite orientations with a 3:1 ratio, and strong overlapping of the $[9]aneS_3$ rings of the two positions. Adding to the poor quality of diffraction data, such disorder hampered an overall anisotropic treatment of the non-hydrogen atoms. For the major component only the Ru, Cl and S atoms were refined anisotropically, with the lighter atoms being included in the final structural model using independent isotropic parameters. For the minor component only the Ru1 atom could be refined using anisotropic parameters, with common isotropic displacement parameters for C and S atoms being used. Additionally, geometric restrictions had to be applied to the minor component to make it structurally similar to the major component (using, for example, the command SAME in SHELXL). In spite of the high disorder for the metal complex, the water molecules of crystallization and the isolated chloride anion were located in well-defined positions, and the assignment of anisotropic displacement parameters for these entities contributed to a considerable improvement on the quality of refinement. Hydrogen atoms bound to carbon were placed at their idealised positions using appropriate *HFIX* instructions in SHELXL: *23* for the $–CH_2–$ methylene and *43* for the CH groups of the aromatic rings. All these atoms were included in subsequent refinement cycles in riding motion approximation with isotropic thermal displacements parameters (U_{iso}) fixed at $1.2 \times U_{eq}$ of the parent carbon atoms. The assignment of hydrogen atoms of the water molecules and the secondary N atoms did not converge to chemically acceptable solutions. These atoms were, however, included in the empirical formula of the compound (Table 1).

The last difference Fourier map synthesis showed the highest peak (0.824 $eÅ^{-3}$) and the lowest hole (-1.601 $eÅ^{-3}$) located at 0.52 Å from C15_1 and 1.28 Å from N2_1, respectively.

Thermal denaturation of salmon sperm DNA

The thermal denaturation temperature of salmon sperm DNA (*s*DNA) and of the mixture **1**/*s*DNA (1:10) was determined in a 10 mM phosphate buffer saline solution (PBS, composition $Na_2HPO_4/NaHPO_4$, pH = 7.4) prepared with ultra-pure water, containing 1.5×10^{-4} M of *s*DNA and 1.5×10^{-5} M of **1**. Melting curves were recorded at 260 nm with samples being heated in steps of ca. 5 °C with 10 min interval between each step. For each temperature point, five absorbance readings were collected and these were averaged before plotting. The melting temperature is defined as the temperature at which 50% of the DNA denaturates into a single strand, and it is obtained from the middle point of the meting curve (represented in the Fig. 7).

The concentration of the stock solution of *s*DNA (prepared by dissolution of 5.13×10^{-7} g in 5 mL of PBS) was determined by spectrophotometry, using the molar extinction coefficient $\varepsilon_{260\ nm} = 6600\ M^{-1}\ cm^{-1}$ (Fasman 1975), to afford a value of [DNA] = 356 M. Furthermore, the solution of *s*DNA gave a ratio of UV absorbance at $A_{260\ nm}/A_{280\ nm}$ of ca. 1.90, indicating that the *s*DNA was sufficiently free of protein (Marmur 1961).

Cell viability studies using the MTT assay

Compounds **1**–**3** were tested against the human MG-63 cell line (osteosarcoma). Their cytotoxicity was assessed by the mitochondrial dehydrogenase activity assay or MTT colorimetric assay (Mosmann 1983), which is based on the ability of tetrazolium dye to form an insoluble coloured compound upon reduction by the intracellular mitochondrial dehydrogenases. Experimental details for the assays are given in the subsections below.

(Note that the evaluation of the IC_{50} values for the complexes analogue to **1** constitutes a secondary aspect of this work, carried out with the aim of a better framing of the activity of the complex **1**; this way, the description of the experimental procedure for the cytotoxicity studies with these complexes is given in the ESI.)

Cell culture procedures

The MG-63 cell line (human osteosarcoma) was kindly provided by the Associate Laboratory IBMC-INEB, Portugal. Cells from this line were cultured in MEM supplemented with 10% heat-inactivated foetal bovine serum (FBS), non-essential amino acids (1 mM), penicillin (100 units/mL), streptomycin (μg/mL) and sodium pyruvate (1 mM) in 75 cm^2 tissue culture flasks at 37 °C in a humidified atmosphere with 5% CO_2. MG-63 were grown in monolayers, sub-cultured every 2–3 days and harvested upon addition of trypsin/EDTA (0.05% trypsin/EDTA solution).

Growth inhibition assays

PBS solutions of the compounds **1**–**3** at concentrations of 1, 2, 3 at 25, 50, 75 and 100 μM were prepared by dissolving them directly into the buffer, because the compounds are water soluble. MTT was prepared in a concentration of 5 mg/mL in PBS. All solutions were sterilised by filtration.

Cell viability following exposure of the MG-63 to each test compound was assessed for only one time point (72 h of incubation). Three independent experiments with triplicates for each drug concentration were performed. MG-63 cells were plated at a density of 2.5 × 104 cells cm^{-2} in 48-well microplates. Twenty-four hours after seeding, test solutions

of **1**, **2** and **3** were added to the medium and cultures were incubated at 37 °C. After an incubation period of 72 h, 55 μL of MTT were added to each well and the plates were incubated at 37 °C for 2 h, after which time MTT was removed by aspiration, and the purple formazan crystals formed in the cells were dissolved by addition of 200 μL of DMSO under stirring. The optical density was measured in microplate reader, at a working wavelength of 570 nm.

Statistical analysis

Experiments for the MG-63 cell line were performed in triplicate. Results are expressed as a percentage of the control (100%) and represent the mean values ± standard deviation (the corresponding error bars are displayed in the graphical plots). Statistical analysis was performed by ANOVA. The Dunnett's post hoc test was used for statistical comparison between the experimental data, p values <0.05 being considered as significant.

Results and discussion

Crystal structure description of $[([9]aneS_3)Ru^{II}(dipa)Cl]Cl{\cdot}3.5H_2O$

The crystal structure of the complex cation $[([9]aneS_3)Ru^{II}(dipa)Cl]^+$ (dipa = di(2-pyridyl)amine, $[9]aneS_3$ = 1,4,7-trithiacyclonane) with hexafluorophosphate, PF_6^-, as the counter-ion, was described previously (Madureira et al. 2000). However, this salt is basically a precursor of complex **1**. Precipitation with PF_6^- allows a quick, high-yield and high purity precipitation of the complex cation which then is converted to its chloride salt (compatible with biological applications since chloride is a physiological anion). It is thus relevant to know the structure of the complex in use in this work, $[([9]aneS_3)Ru^{II}(dipa)Cl]Cl$ (**1**).

The complex **1** crystallises in the orthorhombic space group *Iba2*, with the asymmetric unit being composed by a whole cationic complex molecular unit, $[([9]aneS_3)Ru^{II}(dipa)Cl]^+$, a charge balancing chloride anion and 3.5 water molecules of crystallization. The complex cation is disordered, in a 3:1 proportion, over two different locations with opposite orientations, with high overlapping of the $[9]aneS_3$ macrocycles. In the major component, the coordination environment around the metal centre is close to octahedral, with the Ru–S distances ranging from 2.272(6) to 2.301(4) Å, and the two Ru–N and one R–Cl distances being 2.109(12), 2.149(11) and 2.441(5) Å, respectively. The *cis* and *trans* octahedral angles fall in the 84.8(4)–94.8(3)° and 177.4(3)–178.75(18)° ranges, respectively (see Table S1 and Fig. 1 for details).

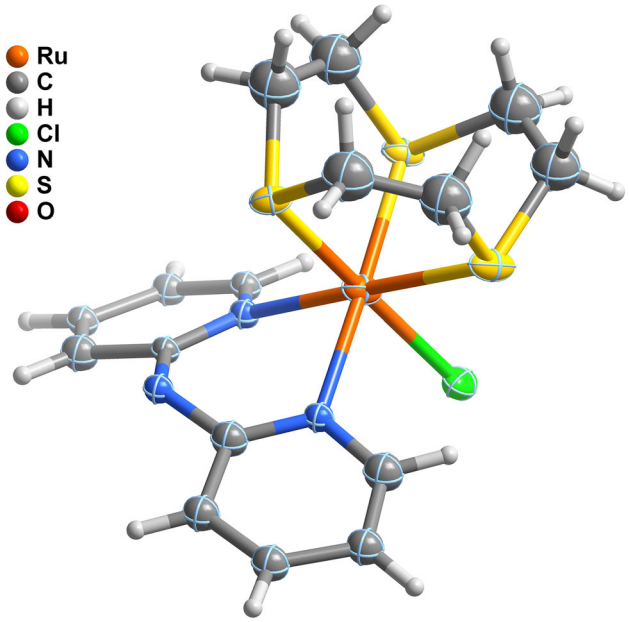

Fig. 1 Schematic representation of the $[([9]aneS_3)Ru^{II}(dipa)Cl]^+$ cationic complex present in the crystal structure with an occupancy of 75%. Non-hydrogen atoms are represented as thermal ellipsoids (for Ru, Cl, and S) or spheres (C and N) drawn at the 50% probability level, while hydrogen atoms are represented as small spheres with arbitrary radii. The hydrogen atom bonded to N2 could not be located. For selected bond lengths and angle ranges referring to the Ru^{2+} coordination sphere please refer to the Table S1 in the Supplementary material

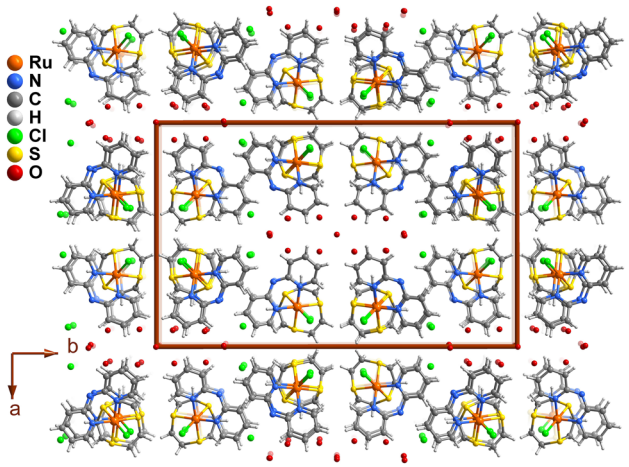

Fig. 2 Crystal packing as seen from the [001] direction of the unit cell of $[([9]aneS_3)Ru^{II}(dipa)Cl]Cl{\cdot}3.5H_2O$ (**1**). For clarity, only the major component of the disordered $[([9]aneS_3)Ru^{II}(dipa)Cl]^+$ cation is depicted. Hydrogen atoms attached to water molecules and atom N2_1 are not shown because they have not been located in the refinement of the crystal structure

The disordered complex cations close pack in columns parallel to the c axis, which are formed, in turn, by four columns related to each other by the glide plans and centred by a twofold rotation axis (see Fig. 2 for details).

β-CD and TRIMEB adducts with 1 and their solid-state characterization

Inclusion of the complex [([9]aneS$_3$)Ru^{II}(dipa)Cl]Cl (**1**) into the CDs followed our previously published adaptations of the co-dissolution procedure, based on the relative solubilities of these hosts (Braga et al. 2001, 2005; Marques et al. 2008, 2009b). β-CD is hydrophilic, and therefore, it dissolves only in water and not in organic solvents. Inclusion was achieved by mixing an aqueous solution of β-CD with an ethanolic solution of **1**, stirring for a short period of 10 min, snap-freezing the mixed solution and then removing the frozen solvent by lyophilisation to obtain compound **2**. The short stirring period aims at minimising the hydrolysis of the chloride ligand in [([9]aneS$_3$)Ru^{II}(dipa)Cl]Cl (**1**). Such procedure was previously proven successful, namely in the preparation of β-CD·Cp$_2$MoCl$_2$ (Braga et al. 2001). The inclusion into TRIMEB, which is soluble in most organic solvents (Petrovski et al. 2005a, b), was carried out in ethanol, allowing to obtain compound **3** quite easily by solvent evaporation. An initial CD/ruthenium complex molar ratio of 1:1 was used for the preparation of the two inclusion compounds, and elemental analysis of **2** and **3** confirmed that the final host:guest molar ratios were close to 1:1.

Vibrational spectroscopy

Preliminary investigations of **2** and **3** using vibrational spectroscopy techniques shows that the structural integrity of the guest was retained during the inclusion procedures. In the FTIR spectra of **2** or **3**, besides the main bands of the hosts (β-CD and TRIMEB, respectively) bands of the guest, [([9]aneS$_3$)Ru^{II}(dipa)Cl]Cl (**1**), are also present. These appear essentially unshifted in **2** and, in the spectrum of **3**, a few bands of the fingerprint spectral region are shifted (Table 2). Raman spectra of the samples **1**–**3** were also collected, with the spectral regions ranging between 250 and 500 cm^{-1} being depicted in the Fig. 3.

The 260–285 cm^{-1} spectral region of **1** presents two bands at 271 and 282 cm^{-1} which can be attributed to RuCl stretching modes by comparison with those of [([9]aneS$_3$)Ru^{II}(bpy)Cl]Cl (found at 282 and 298 cm^{-1}) (Marques et al. 2008). In the same region of the spectra of **2** and **3**, bands ascribed to ν(Ru–Cl) are also observed, thus confirming that the inclusion procedures did not cause hydrolysis of the guest's ruthenium-coordinated chloride. In the 325–425 cm^{-1} spectral region, the Ru–N stretching modes can be observed, additional evidence that the guest's structural integrity is retained with inclusion. Furthermore, one of these bands in **3** is redshifted when compared to that of **1**, suggesting the inclusion of the dipa fragment into the TRIMEB cavity.

Table 2 Selected FTIR bands for compounds **1**–**3**

Selected bands (cm^{-1})			Approximate description
1	**2**	**3**	
271, 282	270, 280	271, 282	ν (Ru–Cl)[a]
320, 340	319, 338	319, 336	ν (Ru–N)
371	370	370	ν (Ru–N) and ν (C–C): py[b]
460, 494	462, 493	462, 495	Ru–pyridine[c]

[a] These bands are assigned to the ν (Ru–Cl) of **1** by Madureira et al. (2000)

[b] As calculated by Chavez-Gil et al. (1998)

[c] By reference to a [Ru(bipy)$_3$]$^{2+}$ mode reported by Riesen et al. (1995)

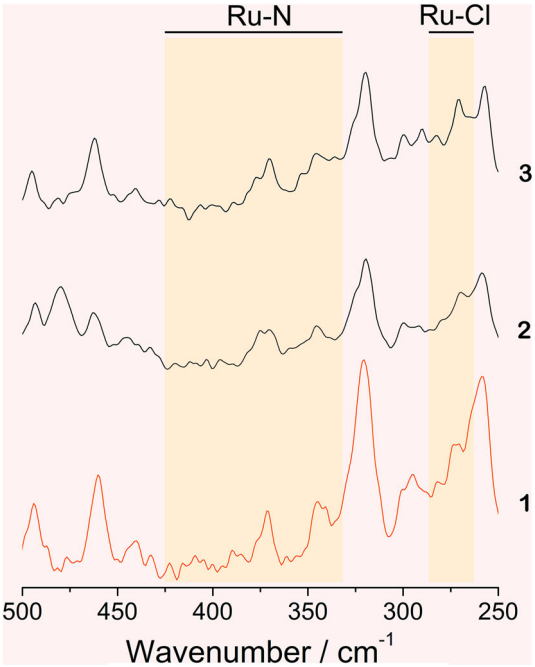

Fig. 3 Raman spectra of the complex **1** and the compounds **2** and **3** in the 500–250 cm^{-1} spectral region. *Shadowed areas* highlight the regions where the Ru–N and Ru–Cl stretching (ν) vibrations occur

Powder X-ray diffraction (PXRD)

PXRD is a helpful technique in the assessment of the purity of the materials. The powder diffractogram of **1** unequivocally confirms that the bulk solid material isolated from its synthesis is isotypical with that of the crystals of **1** (Fig. 4a, b), previously described from single-crystal diffraction studies.

PXRD is also helpful in the study and identification of cyclodextrin inclusion compounds when these appear as new microcrystalline phases (Caira 2001). In the case of **2**, results show that it is mainly amorphous, as noticeable

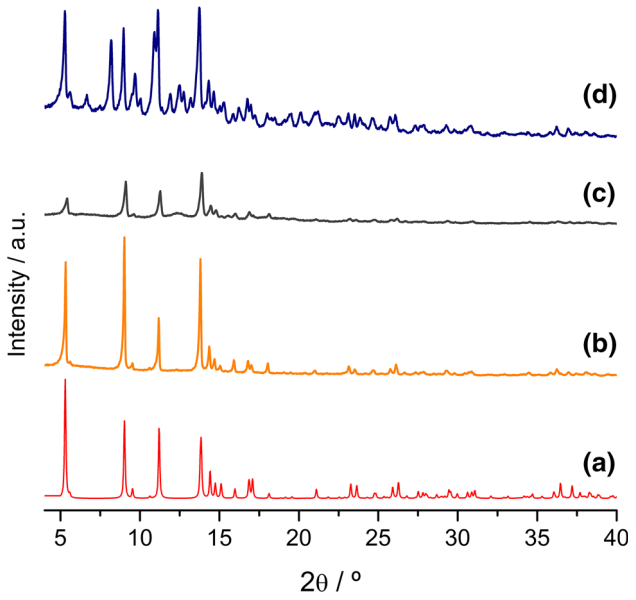

Fig. 4 Experimental and simulated PXRD patterns of **1**–**3**: *a* simulated powder trace of **1** obtained using the coordinates of the crystals of complex **1**; *b* experimental diffraction pattern of **1** as a microcrystalline precipitate; *c* diffractogram of **2**, obtained from co-dissolution with subsequent freeze-drying of **1** and β-CD; *d* diffractogram of **3**, obtained by co-dissolution of **1** and TRIMEB in ethanol followed by vacuum drying

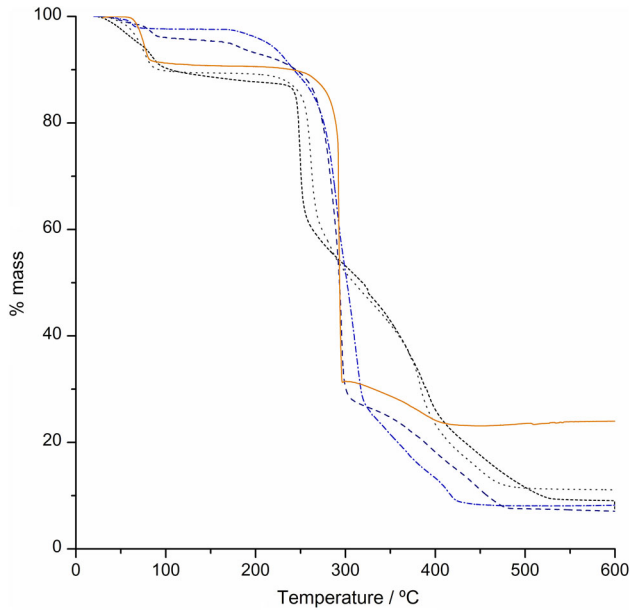

Fig. 5 TG traces for the complex [([9]aneS$_3$)Ru^{II}(dipa)Cl]Cl (**1**) ———, the β-CD adduct (**2**) (— — —), the 1:1 physical mixture of β-CD and **1** (· · · · ·), the TRIMEB adduct (**3**) (— — —), and the 1:1 physical mixture of TRIMEB and **1** (— · — · — ·)

by the presence of a diffraction halo, visible around 13° of 2θ, and it has a minor contamination with microcrystals of the guest. Note that these microcrystals do not alter significantly the properties of **2**, as evidenced by the results from other characterization techniques (namely thermogravimetry, described in the following section). The diffractogram of compound **3** reveals a new phase, which presents, between 7.8 and 10.3 2θ°, a set of three reflections typically associated with TRIMEB inclusion compounds. According to the type of included guest, TRIMEB forms compounds packing in two isostructural series, both belonging to the space group $P2_12_12_1$ (Harata et al. 1998; Brown et al. 1996; Caira et al. 2004a). The first of these series occurs mostly with small guests and features the TRIMEB molecules closely stacked (Caira et al. 2004a). In the second series, which is observed with elongated guest molecules as flurbiprofen, ibuprofen and naproxen, TRIMEB molecules adopt a symmetric, round conformation and pack in antiparallel, head-to-tail channels (Harata et al. 1998; Brown et al. 1996).

Thermogravimetric analysis (TGA)

This tool is quite useful for the recognition of incorporation of a guest into the lattice of a solid inclusion compound. The thermal decomposition profiles of the compounds **1**–**3** are represented in the Fig. 5. The equimolar physical mixtures of **1** with β-CD and TRIMEB were also prepared and the TG traces collected for these samples are presented for comparison. The complex **1** exhibits a dehydration step of ca. 9% from ambient temperature up to about 120 °C, corresponding to 2.7 water molecules, a value which is in fair agreement with the 3.5 hydration waters identified in the single-crystal of **1**. Furthermore, **1** starts to decompose around 270–280 °C, a temperature similar to those of ring decomposition of the cyclodextrins, meaning that the thermogravimetric traces of **2** and **3** follow, in broad terms, those of the mixtures. The presence of inclusion compounds is only discernible by small subtle differences. Concerning **2**, these consist of three main features: (1) the different dehydration profile, (2) a mass loss in the 100–240 °C temperature interval (absent in the mix) and (3) the onset of host decomposition at lower temperature. Mass loss from dehydration in **2** proceeds at two different rates, the first up till 75 °C associated with weakly bound waters and the second (75–100 °C) ascribed to the more tightly bound water molecules, whereas the mixture features a single abrupt step ending at 80 °C. The mass loss from 100 to 240 °C in **2** (c.a. 3%) is common in β-CD inclusion compounds and it is typically ascribed to slow release of the guest molecules (Braga et al. 2001, 2003; Pereira et al. 2007). The third evidence of inclusion is the onset of β-CD decomposition at 240 °C, a lower temperature than those observed for the mix (250 °C) and plain β-

CD hydrate (270 °C, trace not shown). It is attributed to the promoting effects of the ruthenium guest on the decomposition of β-CD as result of a significant host–guest interaction. Co-grinding β-CD and **1** for a few seconds to prepare the physical mixture induced a similar effect due to the strong affinity between these components (Ramos et al. 2013). At 530 °C, **2** exhibits a residual mass of 9.4%, which is comparable to that of the physical mixture (11.2% at around 490 °C) and confirms the 1:1 stoichiometry determined by microanalysis. Note also that no step attributed to the pure complex **1** is observed in the TG trace of **2**, thus showing that the reflections observed in powder XRD are caused by trace amounts of **1**.

Compound **3** has also a distinct thermal decomposition when compared to the mixture, namely in the presence of more hydration waters, also evaporating in two steps (4.5 water molecules up to ca. 96 °C), while dehydration in the mixture occurs in a single abrupt step and ends at ca. 75 °C (2.5 water molecules). Similarly to **2**, compound **3** presents a small and gradual mass loss of 3% in the 96–220 °C temperature range which is not observed in the mixture and can be ascribed to the sublimation of a few guest molecules. Decomposition of TRIMEB starts around 200 °C both in **3** and the mixture.

$^{13}C\{^1H\}$ CP/MAS NMR spectroscopy

The solid-state NMR spectra of **1**, the pure CDs and of **2** and **3** are depicted in the Fig. 6. The complex [([9]aneS$_3$)Ru^{II}(dipa)Cl]Cl (Fig. 6a) presents two resonances for each pyridyl carbon atom, thus evidencing asymmetry in the dipa ligand. In the region of the trithiacyclononane carbons, broad and poorly resolved signals are observed, the most intense centred around 34 ppm and two small shoulders on each side (at roughly 39 and 30 ppm, respectively). The two hosts (β-CD and TRIMEB) exhibit multiple sharp resonances for each type of carbon atom, associated with different torsion angles about the α(1→4) linkages (Gidley and Bociek 1988; Heyes et al. 1992) and with torsion angles describing the orientation of the hydroxyl groups (Veregin et al. 1987) of β-CD, and, in the case of TRIMEB, with a strongly collapsed ring conformation by inversion of one glucose unit to the $^1C_4$ conformation (occurring in TRIMEB monohydrate) and with an overall asymmetry of glucose units due to inclusion of two primary methoxy groups from a neighbouring molecule (observed for TRIMEB anhydrate) (Caira et al. 2004b).

In the spectrum of **2** (Fig. 6c), the host carbon resonances appear as broad signals with little or no structure, which is most likely associated with the loss of crystallinity of the β-CD host evidenced by powder diffraction. The $C_{2,3,5}$ carbons give rise to a large band centred around

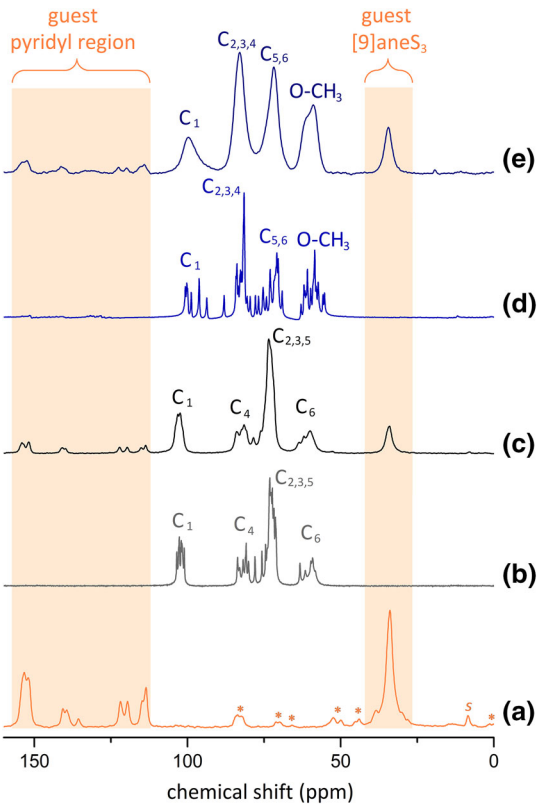

Fig. 6 $^{13}C\{^1H\}$ CP/MAS spectra for *a* the complex **1**, *b* the β-CD host, *c* adduct **2**, *d* TRIMEB and *e* adduct **3**. Spinning sidebands are denoted by *asterisks*, *s* denotes residual solvent

81 ppm, the C_4 and the C_6 carbons appear as poorly resolved multiplets in the 73–11 and 61–11 ppm intervals, respectively, and the resonances for the C_1 carbons of β-CD are represented by a set of two poorly resolved broad peaks around 102.9 and 101.9 ppm. The carbon resonances of the guest appear mostly unshifted. The host carbon signals in compound **3** suffer some modifications, appearing as single featureless signals, as a result of the formation of the inclusion compound. The inclusion of **1**, a relatively large guest molecule, into the cavity of TRIMEB, induces the ring to adopt a more symmetrical conformation (as described previously in the powder X-ray diffraction section), thus resulting in the reduction of the multiplicity of the carbon resonances.

Biological activity assessment

Melting temperature of sDNA

This study provides evidence for the intercalation of small molecules into the DNA double helix, measurable from the increase of the DNA melting temperature (T_m), i.e., the mean temperature at which double stranded DNA

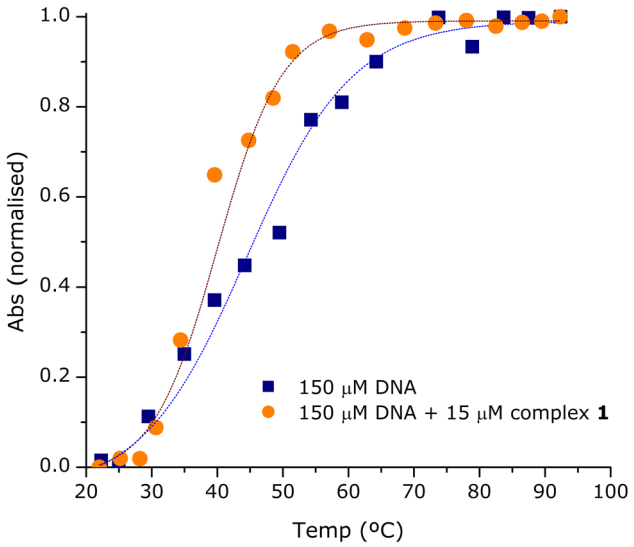

Fig. 7 Comparison of the thermal denaturation curves for (A260 vs. temperature) for pure *s*DNA and the mixture *s*DNA/complex **1** using a 10:1 molar ratio

denatures into single stranded DNA. The melting curves of salmon sperm DNA (*s*DNA) in the absence and presence of the Ru(II) complex **1** are shown in the Fig. 7. Under our experimental conditions, the T_m value of *s*DNA (100 μM in Tris buffer, see experimental section for details) was found to lie around 50 °C. However, in the presence of the complex **1**, at a concentration ratio of [*s*DNA]/[**1**] = 10:1, the melting temperature was lower. The occurrence of a negative value for the ΔT_m is less usual but not unprecedented. A ΔT_m of −2 °C was reported for the complex cation $[(\eta^6\text{-}C_6H_6)RuCl(en)]^+$ (en = ethylenediamine), which preferentially coordinates DNA guanine bases at their endocyclic N7 atoms (Morris et al. 2001). Negative values of ΔT_m are also reported for $[(\eta^5\text{-}C^5Me^5)\text{-}RhCl(L)](CF_3SO_3)$ (L = ethylenediamine, 2,2′-bipyridine, 1,10-phenanthroline), which can potentially bind to the nucleobase N atoms of the DNA (Scharwitz et al. 2008).

Growth inhibition of MG-63 cells at 72 h of incubation

The toxicity of compounds **1–3** was studied by the in vitro MTT assay [22] on a human bone cancer line of interest to our group, the osteosarcoma MG-63 line. The cells were incubated for a period of 72 h with solutions of these compounds in MEM at different concentrations, ranging from 25 to 100 μM (Fig. 8). The pure cyclodextrins (β-CD and TRIMEB) have been previously tested against this cell line and exhibited no intrinsic growth inhibitory action [31]. The complex **1** exhibits a very small (ca. 8%) cell growth inhibition at the concentrations of 50 and 100 μM, which is also observed with 100 μM of the inclusion compound **3**, but these are not considered statistically

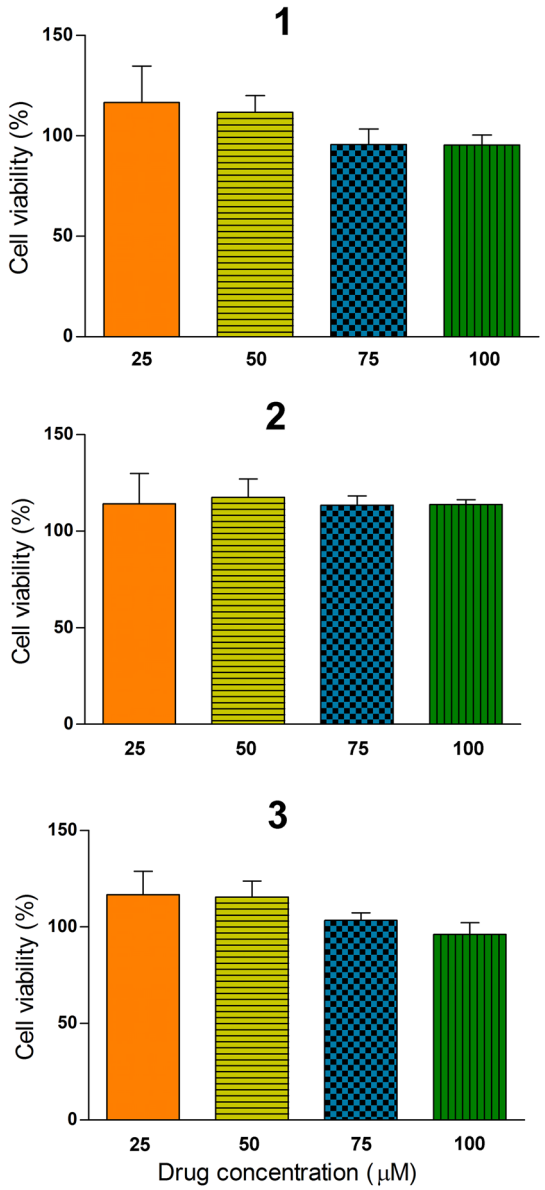

Fig. 8 Cytotoxicity of complex **1** and adducts **2** and **3** against the human osteosarcoma MG-63 cell line, for concentrations ranging from 25 to 100 μM at 72 h incubation. Data are expressed as a percentage of the control (100%) and represent the average ± mean standard deviation from three independent ($n = 3$) experiments carried out in triplicate

significant (p values ≥0.05). Compound **2** had no effect on the growth of MG-63 cells at the tested concentrations.

To better understand whether the non-planarity of the ligand dipa is hampering the activity of the complex **1**, cytotoxic activities can be compared with those of related Ru(II)-trithiacyclononane complexes bearing planar aromatic ligands, namely 2,2′-bipyridine (bpy) and ligands with more extended aromatic fused ring systems such as 1,10-phenanthroline (phen) and dipyrido[3,2-a:2′,3′-c]phenazine (dppz). The later is a well-known DNA-

intercalating planar ligand. Other tumor cell-lines are also included in this expanded analysis (details in the Electronic Supplementary Information, section S2). It is interesting to note that the use of the intercalating ligand dppz (Santos et al. 2001), expected to bring strong biological activity, did not meet the expectations at all. The complex [([9]aneS$_3$)Ru^{II}(dppz)Cl]Cl was inactive against osteosarcoma (MG-63) and presented only mild activity on a breast cancer line (MDA-MB-231). Indeed, all the tested complexes had high IC_{50} values against the osteosarcoma MG-63 line, suggesting that they are not entering the cells in sufficient amounts, being thus unable to reach the nucleus to interact with the DNA.

Conclusions

The present work reports, for the first time, the crystalline structure of the chloride salt of [([9]aneS$_3$)Ru^{II}(dipa)Cl]$^+$ (**1**) and it confirms, by powder diffraction analysis, that the collected crystal is isostructural with the bulk microcrystalline solids (**1**) that are formed in the reported synthetic procedure.

The interaction of **1** with β-CD and TRIMEB is analysed in the solid-state using TGA, powder XRD, $^{13}C\{^1H\}$ CP/MAS NMR and elemental analysis. The products have stoichiometries close to 1:1. The adduct formed with β-CD, named **2**, is mainly amorphous, in a good parallel with β-CD·[([9]aneS$_3$)Ru^{II}(2,2′-bipyridine)Cl]Cl (Marques et al. 2008) in which β-CD interacts with a structurally similar metal guest. The inclusion compound formed with the methylated CD—TRIMEB·[([9]aneS$_3$)Ru^{II}(dipa)Cl]Cl·5H$_2$O (**3**)—presents a fair degree of crystallinity. A careful analysis of the powder diffractogram of **3** has allowed us to postulate that TRIMEB molecules are presumably arranged in infinite channels, typical of TRIMEB inclusion compounds reported for medium-sized guest molecules (Harata et al. 1998). Noteworthy, the structure of TRIMEB·[([9]aneS$_3$)Ru^{II}(2,2′-bipyridine)Cl]Cl, determined by running a Monte Carlo structural optimization on powder X-ray data, is also described as having TRIMEB molecules packed in tilted channels aligned along the crystallographic *c* axis (Marques et al. 2008).

The complex **1** lowers the temperature of denaturation of DNA, which suggests interaction, as reported for other complexes of ruthenium (Morris et al. 2001) and rhenium (Scharwitz et al. 2008). Nevertheless, this interaction is insufficient to warrant a significant cytotoxic action against human osteosarcoma MG-63 cells, either for **1** or for the compounds **2** and **3**. A comparison with other ruthenium trithiacyclononane complexes, including one with dppz, a DNA-intercalating ligand, shows that structural factors of these ligands are not the cause of low cytotoxicity. Alternatively, it may be caused by inability of the complexes in accessing the cell nucleus or by other factors associated with chemotherapy-resistance of the MG-63 cells (Lou et al. 2010). The solution may thus not lie in targeting DNA, but rather in identifying other relevant cellular targets in osteosarcoma cells. Current investigation in the field suggests the Wnt signalling pathway (Guo et al. 2007), the aurora kinase A (AURKA) (Jiang et al. 2014), and the Rho-associated coil containing protein kinase 1 (ROCK1) (Liu et al. 2011) as promising new targets for the inhibition of osteosarcoma growth and/or progression.

Acknowledgements The supply of β-CD (Kleptose) by Roquette Laboratoires (Lestrem, France) is gracefully acknowledged. Thanks are due to Lúcia Anjo for her collaboration in the early steps of the work. We are also grateful to the University of Aveiro and to FCT/MEC (Fundação para a Ciência e a Tecnologia, Ministério da Educação e da Ciência), through national founds and, where applicable, co-financed by the FEDER (European Fund for Regional Development) within the PT2020 Partnership Agreement, for the financial support to the QOPNA research project (FCT UID/QUI/00062/2013), to the Portuguese NMR Network, to CICECO-Aveiro Institute of Materials (FCT UID/CTM/50011/2013), and for specific funding towards the purchase of the single-crystal diffractometer. J.A.F. participated in this work while receiving a post-doctoral grant (SFRH/BPD/63736/2009) supported by the programme POPH (FCT/European Social Fund).

References

Aird RE, Cummings J, Ritchie AA, Muir M, Morris RE, Chen H, Sadler PJ, Jodrell DI (2002) In vitro and in vivo activity and cross resistance profiles of novel ruthenium (II) organometallic arene complexes in human ovarian cancer. Br J Cancer 86:1652–1657. doi:10.1038/sj.bjc.6600290

Allardyce CS, Dyson PJ (2016) Metal-based drugs that break the rules. Dalton Trans 45:3201–3209. doi:10.1039/c5dt03919c

APEX2 (2006) Data collection software version 2.1-RC13. Bruker AXS, Delft

Bergamo A, Masi A, Peacock AF, Habtemariam A, Sadler PJ, Sava G (2010) In vivo tumour and metastasis reduction and in vitro effects on invasion assays of the ruthenium RM175 and osmium AFAP51 organometallics in the mammary cancer model. J Inorg Biochem 104:79–86. doi:10.1016/j.jinorgbio.2009.10.005

Bergamo A, Gaiddon C, Schellens JHM, Beijnen JH, Sava G (2012) Approaching tumour therapy beyond platinum drugs: status of the art and perspectives of ruthenium drug candidates. J Inorg Biochem 106:90–99. doi:10.1016/j.jinorgbio.2011.09.030

Biwer A, Antranikian G, Heinzle E (2002) Enzymatic production of cyclodextrins. Appl Microbiol Biotechnol 59:609–617. doi:10.1007/s00253-002-1057-x

Braga SS, Gonçalves IM, Pillinger M, Ribeiro-Claro P, Teixeira-Dias JJC (2001) Experimental and theoretical study of the interaction of molybdenocene dichloride (Cp_2MoCl_2) with β-cyclodextrin. J Organomet Chem 632:11–16. doi:10.1016/S0022-328X(01)00836-1

Braga SS, Gonçalves IM, Herdtweck E, Teixeira-Dias JJC (2003) Solid state inclusion compound of *S*-ibuprofen in β-cyclodextrin: structure and characterisation. New J Chem 27:597–601. doi:10.1039/B207272F

Braga SS, Marques MPM, Sousa JB, Pillinger M, Teixeira-Dias JJC, Gonçalves IS (2005) Inclusion of molybdenocene dichloride (Cp_2MoCl_2) in 2-hydroxypropyl- and trimethyl-β-cyclodextrin: structural and biological properties. J Organomet Chem 690:2905–2912. doi:10.1016/j.jorganchem.2005.03.012

Braga SS, Coelho AC, Gonçalves IM, Santos G, Fonseca FJ, Andrade AM, Peres M, Simões W, Monteiro T, Pereira L (2008) Luminescence properties of the TRIMEB inclusion compound of a europium tris-β-diketonate. J Non-Cryst Solids 354:2736–2739. doi:10.1016/j.jnoncrysol.2007.09.053

Braga SS, Mokal V, Paz FAA, Pillinger M, Branco A, Sardão VA, Diogo CA, Oliveira PJ, Marques MPM, Romão CC, Gonçalves IM (2014) Synthesis, characterisation and antiproliferative studies of allyl(dicarbonyl)(cyclopentadienyl)molybdenum complexes and cyclodextrin inclusion compounds. Eur J Inorg Chem 2014:5034–5045. doi:10.1002/ejic.201402540

Brown GR, Caira MR, Nassimbeni NL, Van Oudtshoorn B (1996) Inclusion of ibuprofen by heptakis(2,3,6-tri-O-methyl)-β-cyclodextrin: an X-ray diffraction and thermal analysis study. J Incl Phenom Mol Recognit Chem 26:281–294. doi:10.1007/BF01053545

Caira MR (2001) On the isostrucurality of cyclodextrin inclusion complexes and its practical utility. Rev Roum Chim 46:371–386

Caira MR, Giordano F, Vilakazi SL (2004a) X-ray structure and thermal properties of a 1:1 inclusion complex between permethylated β-cyclodextrin and psoralen. Supramol Chem 16:389–393. doi:10.1080/10610270410001713321

Caira MR, Bourne SA, Mhlongo WT, Dean PM (2004b) New crystalline forms of permethylated beta-cyclodextrin. Chem Commun 10(19):2216–2217. doi:10.1039/b408660k

Casarsa C, Mischis MT, Sava G (2004) TGFβ1 regulation and collagen-release-independent connective tissue re-modelling by the ruthenium complex NAMI-A in solid tumours. J Inorg Biochem 98:1648–1654. doi:10.1016/j.jinorgbio.2004.04.017

Charoenlap N, Dharmsthiti S, Sarote S, Sittiwat L (2004) Optimization of cyclodextrin production from sago starch. Bioresour Technol 92:49–54. doi:10.1016/j.biortech.2003.07.007

Chavez-Gil TE, De Faria DLA, Toma HE (1998) Resonance Raman investigation of the chromophore centers in an iron(II)-polyimine supermolecule containing four ruthenium(II)-bipyridine groups. Vib Spectrosc 16:89–92. doi:10.1016/S0924-2031(97)00048-9

Chen H, Wang X, Qi Y, Zheng S, Chen Q, He PG, Zhang F, Yang F, Tang J, Fang Y (2013) A tris(bipyridine)ruthenium(II)–β-cyclodextrin derivative: synthesis, luminescent properties, and application in electrochemiluminescence DNA sensors. ChemPlusChem 78:780–784. doi:10.1002/cplu.201300071

Clarke MJ (1980) Oncological implications of the chemistry of ruthenium. In: Sigel H (ed) Metal ions in biological systems, vol 11. Marcel Dekker, New York, pp 231–283

Clarke MJ (2003) Ruthenium metallopharmaceuticals. Coord Chem Rev 236:209–233. doi:10.1016/S0010-8545(02)00025-5

Cryopad (2006) Remote monitoring and control, Version 1.451. Oxford Cryosystems, Oxford

SAINT+, Data integration engine v. 7.23a ©(1997–2005). Bruker AXS, Madison

Dwyer FP, Gyarfas EC, Rogers WP, Koch JH (1952) Biological activity of complex ions. Nature 170:190–191. doi:10.1038/170190a0

Dwyer FP, Mayhew E, Roe EMF, Shulman A (1965) Inhibition of Landschütz ascites tumour growth by metal chelates derived from 3,4,7,8-tetramethyl-1,10-phenanthroline. Br J Cancer 19:195–199

Dwyer FP, Reid IK, Shulman A, Laycock GM, Dixson S (1969) The biological actions of 1,10-phenanthroline and 2,2′-bipyridine hydrochlorides, quaternary salts and metal chelates and related compounds. 1. Bacteriostatic action on selected gram-positive, gram-negative and acid-fast bacteria. Aust J Exp Biol Med Sci 47:203–218. doi:10.1038/icb.1969.21

Farras P, Waller H, Benniston AC (2016) Enhanced photostability of a ruthenium(II) polypyridyl complex under highly oxidizing aqueous conditions by its partial inclusion into a cyclodextrin. Chem Eur J 22:1133–1140. doi:10.1002/chem.201503485

Fasman GD (1975) Handbook of biochemistry and molecular biology. Nucleic acids, vol 2. CRC Press, Cleveland

Gava B, Zorzet S, Spessotto P, Cocchietto M, Sava G (2006) Inhibition of B16 melanoma metastases with the ruthenium complex imidazolium trans-imidazoledimethylsulfoxide-tetrachlororuthenate and down-regulation of tumor cell invasion. J Pharmacol Exp Ther 317:284–291. doi:10.1124/jpet.105.095141

Gidley MJ, Bociek SM (1988) Carbon-13 CP/MAS NMR studies of amylose inclusion complexes, cyclodextrins, and the amorphous phase of starch granules: relationships between glycosidic linkage conformation and solid-state carbon-13 chemical shifts. J Am Chem Soc 110:3820–3829. doi:10.1021/ja00220a016

Goodfellow BJ, Felix V, Pacheco SMD, De Jesus JP, Drew MGB (1997) Structural characterisation of RuII [9]aneS3 polypyridyl complexes by NMR spectroscopy and single crystal X-ray diffraction. Polyhedron 16:393–401. doi:10.1016/0277-5387(96)00310-5

Guo Y, Zi X, Koontz Z, Kim A, Xie J, Gorlick R, Holcombe RF, Hoang BH (2007) Blocking Wnt/LRP5 signaling by a soluble receptor modulates the epithelial to mesenchymal transition and suppresses met and metalloproteinases in osteosarcoma Saos-2 cells. J Orthop Res 25:964–971. doi:10.1002/jor.20356

Hapiot F, Tilloy S, Monflier E (2006) Cyclodextrins as supramolecular hosts for organometallic complexes. Chem Rev 106:767–780. doi:10.1021/cr050576c

Harata K, Uekama K, Imai T, Hirayama F, Otagiri M (1998) Crystal structures of heptakis(2,3,6-tri-*O*-methyl)-beta-cyclodextrin complexes with *R*-flurbiprofen and *S*-flurbiprofen. J Incl Phenom Mol Recogit Chem 6:443–460. doi:10.1007/BF00660743

Hayward RL, Schornagel QC, Tente R, Macpherson JS, Aird RE, Guichard S, Habtemariam A, Sadler P, Jodrell DI (2005) Investigation of the role of Bax, p21/Waf1 and p53 as determinants of cellular responses in HCT116 colorectal cancer cells exposed to the novel cytotoxic ruthenium(II) organometallic agent, RM175. Cancer Chemother Pharmacol 55:577–583. doi:10.1007/s00280-004-0932-9

Henke MM, Richly H, Drescher A, Grubert M, Alex D, Thyssen D, Jaehde U, Scheulen ME, Hilger RA (2009) Pharmacokinetic study of sodium trans-[tetrachlorobis(1H-indazole)-ruthenate (III)]/-indazole hydrochloride (1:1:1) (FFC14A) in patients with solid tumors. Int J Clin Pharmacol Ther 47:58–60

Heyes SJ, Clayden NJ, Dobson CM (1992) ^{13}C-CP/MAS NMR Studies of the cyclomalto-oligosaccharide (cyclodextrin) hydrates. Carbohydr Res 233:1–14. doi:10.1016/S0008-6215(00)90916-9

Iza N, Guerrero-Martinez A, Tardajos G, Ortiz MJ, Palao E, Montoro T, Radulescu A, Dreiss C, Gonzalez-Gaitano G (2015) Using inclusion complexes with cyclodextrins to explore the aggregation behavior of a ruthenium metallosurfactant. Langmuir 31:2677–2688. doi:10.1021/la504929x

Jiang Z, Jiang J, Yang H, Ge Z, Wang Q, Zhang L, Wu C, Wang J (2014) Silencing of Aurora kinase A by RNA interference inhibits tumor growth in human osteosarcoma cells by inducing apoptosis and G2/M cell cycle arrest. Oncol Rep 31:1249–1254. doi:10.3892/or.2014.2986

Kapitza S, Jakupec MA, Uhl M, Keppler BK, Marian B (2005) The heterocyclic ruthenium(III) complex KP1019 (FFC14A) causes DNA damage and oxidative stress in colorectal tumor cells. Cancer Lett 226:115–121. doi:10.1016/j.canlet.2005.01.002

Kottke T, Stalke D (1993) Crystal handling at low temperatures. J Appl Crystallogr 26:615–619. doi:10.1107/S0021889893002018

Landgrafe C, Sheldrick WS (1994) Structure and reactions of the thioether half-sandwich Ruthenium(II) complexes [Ru(MeCN)3([9]aneS$_3$)][CF$_3$SO$_3$]$_2$ and [Ru(MeCN)([9]aneS$_3$)][CF$_3$SO$_3$]$_2$ ([9]aneS = 1,4,7-trithiacyclononane). J Chem Soc Dalton Trans 1994:1885–1893. doi: 10.1039/DT9940001885

Lebron JA, Ostos FJ, Moya ML, Lopez-Lopez MC, Carrasco J, Lopez-Cornejo P (2015) Cooperative interaction between metallosurfactants, derived from the [Ru(2,2′-bpy)$_3$]$^{2+}$ complex, and DNA. Colloid Surf B 135:817–824. doi:10.1016/j.colsurfb.2015.08.052

Leijen S, Burgers SA, Baas P, Pluim D, Tibben M, Van Werkhoven E, Alessio E, Sava G, Beijnen JH, Schellens JHM (2015) Phase I/II study with ruthenium compound NAMI-A and gemcitabine in patients with non-small cell lung cancer after first line therapy. Invest New Drugs 33:201–214. doi:10.1007/s10637-014-0179-1

Lentz F, Drescher A, Lindauer A, Henke M, Hilger RA, Hartinger CG, Scheulen ME, Dittrich C, Keppler BK, Jaehde U (2009) Pharmacokinetics of a novel anticancer ruthenium complex (KP1019, FFC14A) in a phase I dose-escalation study. Anticancer Drugs 20:97–103. doi:10.1097/CAD.0b013e328322fbc5

Liu X, Choi E, Hornicek FJ, Yang S, Yang C, Harmon D, Mankin H, Duan Z (2011) ROCK1 as a potential therapeutic target in osteosarcoma. J Orthop Res 29:1259–1266. doi:10.1002/jor.21403

Lou N, Wang Y, Sun D, Zhao J, Wang Y, Gao Y (2010) Isolation of stem-like cells from human MG-63 osteosarcoma cells using limiting dilution in combination with vincristine selection. Ind J Biochem Biophys 47:340–347

Madureira J, Santos TM, Goodfellow BJ, Lucena M, De Jesus JP, Santana-Marques MG, Drew MGB, Felix V (2000) Structural characterisation of new RuII[9]aneS3 polypyridylic complexes. J Chem Soc Dalton Trans 2000:4422–4431. doi:10.1039/b004752j

Marmur J (1961) A procedure for the isolation of deoxyribonucleic acid from micro-organisms. J Mol Biol 3:208–218. doi:10.1016/S0022-2836(61)80047-8

Marques J, Anjo L, Marques MPM, Santos TM, Paz FAA, Braga SS (2008) Structural studies on supramolecular adducts of cyclodextrins with the complex [Ru([9]aneS$_3$)(bpy)Cl]Cl. J Organomet Chem 693:3021–3028. doi:10.1016/j.jorganchem.2008.06.023

Marques J, Santos TM, Marques MPM, Braga SS (2009a) A glycine ruthenium trithiacyclononane complex and its molecular encapsulation using cyclodextrins. Dalton Trans 2009:9812–9819. doi:10.1039/B915839A

Marques J, Braga TM, Paz FAA, Santos TM, Lopes MFS, Braga SS (2009b) Cyclodextrins improve the antimicrobial activity of the chloride salt of Ruthenium(II) chloro-phenanthroline-trithiacyclononane. Biometals 22:541–556. doi:10.1007/s10534-009-9211-x

Marques J, Fernandes JA, Paz FAA, Marques MPM, Braga SS (2012) Isolation, crystal structure, and cytotoxicity on osteosarcoma of a ruthenium(III) complex with coordinated acetonitrile. J Coord Chem 65:2489–2499. doi:10.1080/00958972.2012.696624

Marques J, Silva VLM, Silva AMS, Marques MPM, Braga SS (2014) Ru(II) trithiacyclononane 5-(2-hydroxyphenyl)-3-[(4-methoxystyryl)pyrazole], a complex with facile synthesis and high cytotoxicity against PC-3 and MDA-MB-231 cells. Complex Metals 1:7–12. doi:10.1080/2164232X.2013.873992

Martin R, Fragoso A, Cao R (2003) Complexation of bis(morpholyldithiocarbamato)copper(II), a superoxide scavenger, in β-cyclodextrins. Supramol Chem 15:171–175. doi:10.1080/1061027031000078266

Mestroni G, Alessio E, Sava G (1996) Nuovi Sali di complessi anionici di rutenio(III), utili in terapia come agenti antimetastatici ed antineoplastici. Ital Pat MI96A001359

Morris RE, Aird RE, Murdoch PS, Chen HM, Cummings J, Hughes ND, Parsons S, Parkin A, Boyd G, Jodrell DI, Sadler PJ (2001) Inhibition of cancer cell growth by ruthenium(II) arene complexes. J Med Chem 44:3616–3621. doi:10.1021/jm010051m

Mosmann T (1983) Rapid colorimetric assay for cellular growth and survival: application to proliferation and cytotoxicity assays. J Immunol Methods 65:55–63. doi:10.1016/0022-1759(83)90303-4

Murray BS, Menin L, Scopelliti R, Dyson PJ (2014) Conformational control of anticancer activity: the application of arene-linked dinuclear ruthenium(II) organometallics. Chem Sci 5:2536–2545. doi:10.1039/c4sc00116h

Murray BS, Babak MV, Hartinger CG, Dyson PJ (2016) The development of RAPTA compounds for the treatment of tumors. Coord Chem Rev 306:86–114. doi:10.1016/j.ccr.2015.06.014

Nardon C, Brustolin L, Fregona D (2016) Is matching ruthenium with dithiocarbamato ligands a potent chemotherapeutic weapon in oncology? Future Med Chem 8:211–226. doi:10.4155/fmc.15.175

Paz FAA, Braga SS (2010) Shaping cytotoxicity of organometallics and complex antitumorals via molecular encapsulation. In: Chin HF (ed) Organometallic compounds: preparation, structure and properties. Nova Science Publishers, Hauppauge, New York pp 465–481

Pereira CCL, Nolasco M, Braga SS, Paz FAA, Ribeiro-Claro P, Pillinger M, Gonçalves IM (2007) A combined theoretical-experimental study of the inclusion of niobocene dichloride in native and permethylated β-cyclodextrins. Organometallics 26:4220–4228. doi:10.1021/om7003749

Peti W, Pieper T, Sommer M, Keppler BK, Giester G (1999) Synthesis of tumor-inhibiting complex salts containing the anion trans-tetrachlorobis(indazole)ruthenate(III) and crystal structure of the tetraphenylphosphonium salt. Eur J Inorg Chem 1999:1551–1555. doi:10.1002/(SICI)1099-0682(199909)1999:9<1551::AID-EJIC1551>3.0.CO;2-7

Petrovski Ž, Braga SS, Rodrigues SS, Pereira CCL, Gonçalves IM, Pillinger M, Freire C, Romão CC (2005a) Synthesis of ferrocenyldiimine metal carbonyl complexes and an investigation of the Mo adduct encapsulated in cyclodextrin. New J Chem 29:347–354. doi:10.1039/B409961C

Petrovski Ž, Braga SS, Santos AM, Rodrigues SS, Gonçalves IM, Pillinger M, Kuhn FE, Romão CC (2005b) Synthesis and characterization of the inclusion compound of a ferrocenyldiimine dioxomolybdenum complex with heptakis-2,3,6-tri-O-methyl-β-cyclodextrin. Inorg Chim Acta 358:981–988. doi:10.1016/j.ica.2004.11.032

Pirvu CD, Aramă CC, Radu C, Uivarosi V (2013) Preliminary preformulation studies for a new norfloxacin ruthenium (III) complex with biological activity. Farmacia 61:251–261. Available online at: http://www.revistafarmacia.ro/201302/art-03-pirvu251-261.pdf

Prochowicz D, Kornowicz A, Justyniak I, Lewinski J (2016) Metal complexes based on native cyclodextrins: synthesis and structural diversity. Coord Chem Rev 306:331–345. doi:10.1016/j.ccr.2015.07.016

Ramos AI, Braga TM, Silva P, Fernandes JA, Ribeiro-Claro P, Lopes MFS, Paz FAA, Braga SS (2013) Chloramphenicol·cyclodextrin inclusion compounds: co-dissolution and mechanochemical preparations and antibacterial action. CrystEngComm 15:2822–2834. doi:10.1039/C3CE26414A

Riesen H, Wallace L, Krausz E (1995) Vibrational sidelines in the localized ^{3}MLCT luminescence of [Ru(bpy)$_{3-x}$(L)$_x$]$^{2+}$ ($x = 0$ *to* 3, L = 3,3′-bipyridazine, bpy-d_8) in the C2/c [Zn(bpy)$_3$](ClO$_4$)$_2$

lattice. Chem Phys 198:269–280. doi:10.1016/0301-0104(95)00190-Y

Rilak A, Bratsos I, Zangrando E, Kljun J, Turel I, Bugarčić ŽD, Alessio E (2014) New water-soluble ruthenium(II) terpyridine complexes for anticancer activity: synthesis, characterization, activation kinetics, and interaction with guanine derivatives. Inorg Chem 53:6113–6126. doi:10.1021/ic5005215

Romain C, Gaillard S, Elmkaddem MK, Toupet L, Fischmeister C, Thomas CM, Renaud JL (2010) New dipyridylamine ruthenium complexes for transfer hydrogenation of aryl ketones in water. Organometallics 29:1992–1995. doi:10.1021/om100127f

Santos TM, Madureira J, Goodfellow BJ, Drew MGB, De Jesus JP, Felix V (2001) Interaction of ruthenium(II)-dipyridophenazine complexes with CT-DNA: effects of the polythioether ancillary ligands. Met Based Drugs 8(2001):125–136. doi:10.1155/MBD.2001.125

Sava G, Capozzi I, Clerici K, Gagliardi G, Alessio E, Mestroni G (1998) Pharmacological control of lung metastases of solid tumours by a novel ruthenium complex. Clin Exp Metastasis 16:371–379. doi:10.1023/A:1006521715400

Sava G, Zorzet S, Turrin C, Vita F, Soranzo M, Zabucchi G, Cocchietto M, Bergamo A, DiGiovine S, Pezzoni G, Sartor L, Garbisa S (2003) Dual action of NAMI-A in inhibition of solid tumor metastasis: selective targeting of metastatic cells and binding to collagen. Clin Cancer Res 9:1898–1905

Sava G, Frausin F, Cocchietto M, Vita F, Podda E, Spessotto P, Furlani A, Scarcia V, Zabucchi G (2004) Actin-dependent tumour cell adhesion after short-term exposure to the antimetastasis ruthenium complex NAMI-A. Eur J Cancer 40:1383–1396. doi:10.1016/j.ejca.2004.01.034

Scharwitz MA, Ott I, Geldmacher Y, Gust R, Sheldrick WS (2008) Cytotoxic half-sandwich rhodium(III) complexes: polypyridyl ligand influence on their DNA binding properties and cellular uptake. J Organomet Chem 693:2299–2309. doi:10.1016/j.jorganchem.2008.04.002

Scolaro C, Hartinger CG, Allardyce CS, Keppler BK, Dyson PJ (2008) Hydrolysis study of the bifunctional antitumour compound RAPTA-C, [Ru(η^6-*p*-cymene)Cl_2(pta)]. J Inorg Biochem 102:1743–1748. doi:10.1016/j.jinorgbio.2008.05.004

Sheldrick GM (1997a) SHELXS-97, program for crystal structure solution. University of Gottingen, Gottingen

Sheldrick GM (1997b) SHELXL-97, program for crystal structure refinement. University of Gottingen, Gottingen

Sheldrick GM (1998) SADABS v.2.01, Bruker/Siemens Area Detector Absorption Correction Program. Bruker AXS, Madison

Sheldrick GM (2008) A short history of SHELX. Acta Cryst A 64:112–122. doi:10.1107/S0108767307043930

Szerman N, Schroh I, Rossi AL, Rosso AM, Krymkiewicz N, Ferrarotti SA (2007) Cyclodextrin production by cyclodextrin glycosyltransferase from *Bacillus circulans* DF 9R. Biores Technol 98:2886–2891. doi:10.1016/j.biortech.2006.09.056

Veregin RP, Fyfe CA, Marchessault RH, Taylor MG (1987) Correlation of ^{13}C chemical-shifts with torsional angles from high-resolution, ^{13}C-CP-MAS NMR studies of crystalline cyclomalto-oligosaccharide complexes, and their relation to the structures of the starch polymorphs. Carbohydr Res 160:41–56. doi:10.1016/0008-6215(87)80302-6

Zhang F, Zhao YY, Chen H, Wang XH, Chen Q, He PG (2015) Sensitive fluorescence detection of lysozyme using a tris(bipyridine)ruthenium(II) complex containing multiple cyclodextrins. Chem Commun 51:6613–6616. doi:10.1039/C5CC00428D